A Modified Distributed Lagrange Multiplier/Fictitious Domain Method for Particulate Flows with Collisions

P. Singh
Department of Mechanical Engineering
New Jersey Institute of Technology
University Heights
Newark, NJ 07102

T.I. Hesla and D.D. Joseph
Department of Aerospace Engineering and Mechanics
University of Minnesota
Minneapolis, MN 55455

A modified distributed Lagrange multiplier/fictitious domain method (DLM) that allows particles to undergo collisions is developed for particulate flows. In the earlier versions of the DLM method for Newtonian and viscoelastic liquids described in [1,2] the particle surfaces were restricted to be at least one and half times the velocity element size away from each other. A repulsive body force was applied to the particles when the distance between them was smaller than this critical value. This was necessary for ensuring that conflicting rigid body motion constraints from two different particles are not imposed at the same velocity nodes.

In the modified DLM method the particles are allowed to come arbitrarily close to each other and even slightly overlap each other. When conflicting rigid body motion constraints from two different particles are applicable on a velocity node, the constraint from the particle that is closer to that node is used and the other constraint is dropped. An elastic repulsive force is applied when the particles overlap each other. In our simulations, the particles are allowed to overlap as much as one hundredth of the velocity element size. The modified DLM method is implemented for both Newtonian and viscoelastic liquids.

Our simulations show that when particles are dropped in a channel, and the viscoelastic Mach number (M) is less than one and the elasticity number (E) is greater than one, the particles form a chain parallel to the flow direction. As in experiments, the new method allows particles in the chain to touch each other. The particles dropped in a Newtonian liquid, on the other hand, undergo characteristic drafting kissing and tumbling. During the touching phase, as in experiments, the two particles touch each other. Our results for the time dependent motion of a particle thrown with a given velocity towards the wall or another particle of the same size are in agreement with asymptotic analytical results [3]. We also find good agreement between the analytical and simulations results for a particle sedimenting under gravity onto a horizontal surface.

1. Introduction

Collisions—or near-collisions—between particles present severe difficulties in direct simulations of particulate flows. In point of fact, however, smooth particles cannot actually contact each other in finite time in the continuous system, as shown in Hesla [3][1]. In light of this, the term "collision" is somewhat misleading—at least for smooth particles. However, since the gap width can become exceedingly small in certain situations, numerical truncation errors may allow actual contact (or even overlap) to occur in simulations.

Even near-collisions can greatly increase the cost of a simulation, because in order to simulate the particle-particle interaction mechanism, the flow fields in the narrow gap between the converging particle surfaces must be accurately resolved. The element size required for this decreases with the gap width, leading to extremely small elements and greatly increased numbers of unknowns to be solved for. Actual overlap can lead to overdetermined systems of equations, and must thus be prevented at all costs.

In numerical simulations to date [1,2,4-8], this problem is avoided by introducing an artificial repulsive force between particles which keeps the particle surfaces more than one element apart from each other. In the standard distributed Lagrange multiplier/fictitious domain (DLM) method [1,2,7-8], this ensures that the differing rigid-body motion constraints of the two particles are not simultaneously imposed at any one velocity node, which would lead to a numerically overdetermined system of equations. In the arbitrary Lagrangian-Eulerian (ALE) method [4-6], it ensures that the element size doesn't become excessively small. The ALE method requires two layers of elements in the gap between the converging surfaces.

In this paper, we present a modification of the DLM finite-element scheme described in [1,2] which allows particles to come arbitrarily close to each other, and even overlap slightly. The basic idea is to simply *drop* one of the conflicting rigid-body motion constraint terms in the equation of motion—the one corresponding to the particle surface which is farther away from the node in question. This trick avoids overdetermined systems of equations, but is applicable only as long as the overlap of the particles does not exceed one element. An elastic repulsive force is introduced to prevent particles from overlapping more than that.

---

[1] In actual experiments, one often (apparently) sees collisions. This may be attributed to one or more of the following:

- The particle surfaces are not actually in contact on the microscopic scale.
- The particle surfaces are not actually smooth on the microscopic scale.
- Some new physics comes into play when the gap is extremely narrow.

However, this is irrelevant for the present purposes, since we are simply solving the equations of motion of the fluid and particles, as given by continuum mechanics.

The modified DLM method is verified by comparing the time dependent trajectories for two circular particles falling in a channel for two different mesh refinements, and for two different time steps. It is shown that the results are independent of the mesh resolution and the time step.

It was discussed in [1,2,9,10] that when two or more particles are dropped in a channel filled with a viscoelastic liquid the orientation of particles relative to the direction of flow is determined by the Mach number $M=\sqrt{Re\ De}$ and the elasticity number $E=\frac{De}{Re}$. Here $De=\frac{U\lambda_r}{D}$ is the Deborah number, and $Re=\frac{\rho_L UD}{\eta}$ is the Reynolds number, where λ_r is the relaxation time of the fluid, η is the zero shear viscosity of the fluid, U is the particle velocity, and D is the particle diameter. Specifically, when M is less than one and E is greater than one, the particles align themselves parallel to the flow direction. The distance between the particles of a chain may be very small. In fact, the particles may even approximately touch each other. On the other hand, when these conditions are not satisfied, or when the fluid is Newtonian, the particles undergo drafting kissing and tumbling. Experiments show that during kissing the particles come very close to each other, and may even approximately touch each other.

In the next section the strong and weak forms of governing equations as well as the modified DLM scheme that allows particle-particle near collisions is presented. In the last section, we present several test cases to validate the scheme, and to demonstrate that it performs as advertised.

2. Computational Scheme

The computational scheme we propose is a modification of the DLM finite-element scheme described in [1,2]. In this scheme, the fluid flow equations are solved on the *combined* fluid-solid domain, and the motion inside the particle boundaries is forced to be rigid-body motion using a distributed Lagrange multiplier. The fluid and particle equations of motion are combined into a single combined weak equation of motion, eliminating the hydrodynamic forces and torques, which helps ensure stability of the time integration. The time integration is performed using the Marchuk-Yanenko operator splitting method, which is first-order accurate. See [1,2] for further details.

2.1 Governing Equations

In this paper we will present results for two-dimensional flows. Let us denote the domain containing the Newtonian or viscoelastic fluid and N particles by Ω, and the interior of the ith particle by $P_i(t)$. For simplicity we will assume that the domain is rectangular with boundary Γ. The four sides of the domain will be denoted by Γ_1, Γ_2, Γ_3, and Γ_4 (see Figure 1), and Γ^- will be used to denote the

upstream part of Γ. The viscoelastic fluid is modeled by the Oldroyd-B model. The governing equations for the fluid-particle system are:

$$\rho_L \left[\frac{\partial \mathbf{u}}{\partial t} + \mathbf{u}.\nabla \mathbf{u} \right] = \rho_L \mathbf{g} - \nabla p + \nabla.(\frac{c}{\lambda_r}\mathbf{A}) + \nabla.(2\eta_s \mathbf{D}) \qquad \text{in } \Omega \backslash \overline{P(t)} \qquad (1)$$

$$\nabla \cdot \mathbf{u} = 0 \qquad \text{in } \Omega \backslash \overline{P(t)} \qquad (2)$$

$$\mathbf{u} = \mathbf{u}_L \qquad \text{on } \Gamma \qquad (3)$$

$$\mathbf{u} = \mathbf{U}_i + \omega_i \text{ x } \mathbf{r}_i \qquad \text{on } \partial P_i(t) \text{ , i=1,…,N,} \qquad (4)$$

with the evolution of the configuration tensor **A** given by

$$\frac{\partial \mathbf{A}}{\partial t} + \mathbf{u}.\nabla \mathbf{A} = \mathbf{A}.\nabla \mathbf{u} + \nabla \mathbf{u}^T.\mathbf{A} - \frac{1}{\lambda_r}(\mathbf{A} - \mathbf{I}), \qquad (5)$$

$$\mathbf{A} = \mathbf{A}_L \qquad \text{on } \Gamma^-.$$

Here **u** is the velocity, p is the pressure, η_s is the solvent viscosity, ρ_L is the density, **D** is the symmetric part of the velocity gradient tensor, c is a measure of polymer concentration in terms of the zero shear viscosity, and where λ_r is the relaxation time. The zero shear viscosity $\eta = \eta_s + \eta_p$, where $\eta_p = c\,\eta_s$ is the polymer contribution to viscosity. The fluid retardation time is equal to $\frac{\lambda_r}{1+c}$. The above equations are solved with the following initial conditions:

$$\mathbf{u}|_{t=0} = \mathbf{u}_0 \qquad (6)$$

$$\mathbf{A}|_{t=0} = \mathbf{A}_0 \qquad (7)$$

where $\mathbf{u}_0$ and $\mathbf{A}_0$ are the known initial values of the velocity and the configuration tensor.

The particle velocity $\mathbf{U}_i$ and angular velocity ω_i are governed by

$$M_i \frac{d\mathbf{U}_i}{dt} = M_i \mathbf{g} + \mathbf{F}_i \qquad (8)$$

$$I_i \frac{d\omega_i}{dt} = T_i \qquad (9)$$

$$\mathbf{U}_i|_{t=0} = \mathbf{U}_{i,0} \qquad (10)$$

$$\omega_i|_{t=0} = \omega_{i,0} \qquad (11)$$

where M_i and I_i are the mass and moment of inertia of the ith particle, and $\mathbf{F}_i$ and $\mathbf{T}_i$ are the hydrodynamic force and torque acting on the ith particle. In this investigation we will assume that the particles are circular, and therefore we do not need to keep track of the particle orientation. The particle positions are obtained from

$$\frac{d\mathbf{X}_i}{dt} = \mathbf{U}_i \tag{12}$$

$$\mathbf{X}_i \,|_{t=0} = \mathbf{X}_{i,0} \tag{13}$$

where $X_{i,0}$ is the position of the ith particle at time t=0.

2.2 Weak form of equations and finite-element discretization

The approach used for obtaining the weak form of the governing equations stated in the previous section was described in [1,2,7]. In obtaining this weak form, the hydrodynamic forces and torques acting on the particles can be completely eliminated by combining the fluid and particle equations of motion into a single weak equation of motion for the combined fluid-particle system. For simplicity, in this section we will assume that there is only one particle. The extension to the many-particle case is straightforward.

The solution and variation are required to satisfy the strong form of the constraint of rigid body motion throughout P(t). In the distributed Lagrange multiplier method this constraint is removed from the velocity space and enforced weakly as a side constraint using a distributed Lagrange multiplier term. It was shown in [1,7] that the following weak formulation of the problem holds in the extended domain:

For a.e. t>0, find $\mathbf{u} \in \overline{W}_{u\Gamma}$, $\mathbf{A} \in \overline{W}_A$, $p \in L_0^2(\Omega)$, $\boldsymbol{\lambda} \in \Lambda(t)$, $\mathbf{U} \in \mathbf{R}^2$, and $\omega \in \mathbf{R}$, satisfying

$$\int_\Omega \rho_L \left(\frac{d\mathbf{u}}{dt} - \mathbf{g} \right) \cdot \mathbf{v} d\mathbf{x} - \int_\Omega p \nabla . \mathbf{v} \, d\mathbf{x} + \int_\Omega 2\eta_s \mathbf{D}[\mathbf{u}] : \mathbf{D}[\mathbf{v}] d\mathbf{x} - \int_\Omega \mathbf{v} . \nabla . \left(\frac{c}{\lambda_r} \mathbf{A} \right) d\mathbf{x}$$
$$+ \left(1 - \frac{\rho_L}{\rho_d} \right) \left(M \left(\frac{d\mathbf{U}}{dt} - \mathbf{g} \right) \cdot \mathbf{V} + I \frac{d\omega}{dt} \xi \right) - \mathbf{F}' . \mathbf{V} = \left\langle \boldsymbol{\lambda}, \mathbf{v} - (\mathbf{V} + \xi \times \mathbf{r}) \right\rangle_{P(t)}$$

for all $\mathbf{v} \in \overline{W}_0$, $\mathbf{V} \in \mathbf{R}^2$, and $\xi \in \mathbf{R}$, (14)

$$\int_\Omega q \nabla . \mathbf{u} \, d\mathbf{x} = 0 \qquad \text{for all } q \in L^2(\Omega), \tag{15}$$

$$\left\langle \boldsymbol{\mu}, \mathbf{u} - (\mathbf{U} + \omega \times \mathbf{r}) \right\rangle_{P(t)} = 0 \qquad \text{for all } \boldsymbol{\mu} \in \Lambda(t), \tag{16}$$

$$\int_\Omega \left(\frac{\partial \mathbf{A}}{\partial t} + \mathbf{u} \cdot \nabla \mathbf{A} - \mathbf{A} \cdot \nabla \mathbf{u} - \nabla \mathbf{u}^T \cdot \mathbf{A} + \frac{1}{\lambda_r} (\mathbf{A} - \mathbf{I}) \right) \cdot \mathbf{s} \, d\mathbf{x} = 0 \qquad \text{for all } \mathbf{s} \in \overline{W}_{A0}, \tag{17}$$

$$\mathbf{u} \,|_{t=0} = \mathbf{u}_o \qquad \text{in } \Omega, \tag{18}$$

$$\mathbf{A} \,|_{t=0} = \mathbf{A}_o \qquad \text{in } \Omega, \tag{19}$$

as well as the kinematic equations and the initial conditions for the particle linear and angular velocities. Here **F'** is the additional body force applied to the particles to limit the extent of overlap (see equation (27) below) and $\boldsymbol{\lambda}$ is the distributed Lagrange multiplier

$$\overline{W}_{u\Gamma} = \{\mathbf{v} \in H^1(\Omega)^2 \mid \mathbf{v} = \mathbf{u}_\Gamma(t) \quad \text{on} \quad \Gamma\},$$

$$\overline{W}_0 = H_0^1(\Omega)^2,$$

$$\overline{W}_A = \{\mathbf{A} \in H^1(\Omega)^3 \mid \mathbf{A} = \mathbf{A}_L(t) \quad \text{on} \quad \Gamma^-\},$$

$$\overline{W}_{A0} = \{\mathbf{A} \in H^1(\Omega)^3 \mid \mathbf{A} = 0 \quad \text{on} \quad \Gamma^-\},$$

$$L_0^2(\Omega) = \{q \in L^2(\Omega) \mid \int_\Omega q \, d\mathbf{x} = 0\}, \tag{20}$$

and $\Lambda(t)$ is $L^2(P(t))^2$, with $\langle .,. \rangle_{P(t)}$ denoting the L^2 inner product over the particle, where Γ^- is the upstream part of Γ. In our simulations, since the velocity and $\boldsymbol{\mu}$ are in L^2, we will use the following inner product

$$\langle \boldsymbol{\mu}, \mathbf{v} \rangle_{P(t)} = \int_{P(t)} (\boldsymbol{\mu}.\mathbf{v}) \, d\mathbf{x}. \tag{21}$$

In order to solve the above problem numerically, we will discretize the domain using a regular finite element triangulation T_h for the velocity and configuration tensor, where h is the mesh size, and a regular triangulation T_{2h} for the pressure. The following finite dimensional spaces are defined for approximating $\overline{W}_{u\Gamma}$, $\overline{W}_0$, $\overline{W}_A$, $\overline{W}_{A0}$, $L^2(\Omega)$ and $L_0^2(\Omega)$:

$$W_{u\Gamma,h} = \{\mathbf{v}_h \in C^0(\overline{\Omega})^2 \mid \mathbf{v}_h|_T \in P_1 \times P_1 \text{ for all } T \in T_h, \mathbf{v}_h = \mathbf{u}_{\Gamma,h} \text{ on } \Gamma\},$$

$$W_{0,h} = \{\mathbf{v}_h \in C^0(\overline{\Omega})^2 \mid \mathbf{v}_h|_T \in P_1 \times P_1 \text{ for all } T \in T_h, \mathbf{v}_h = 0 \text{ on } \Gamma\}, \tag{22}$$

$$L_h^2 = \{q_h \in C^0(\overline{\Omega}) \mid q_h|_T \in P_1 \text{ for all } T \in T_{2h}\},$$

$$L_{0,h}^2 = \{q_h \in L_h^2 \mid \int_\Omega q_h \, d\mathbf{x} = 0\}, \tag{23}$$

$$W_{Ah} = \{\mathbf{s}_h \in C^0(\overline{\Omega})^3 \mid \mathbf{s}_h|_T \in P_1 \times P_1 \times P_1 \text{ for all } T \in T_h, \mathbf{s}_h = \mathbf{A}_{L,h} \text{ on } \Gamma^-\},$$

$$W_{A0,h} = \{\mathbf{s}_h \in C^0(\overline{\Omega})^3 \mid \mathbf{s}_h|_T \in P_1 \times P_1 \times P_1 \text{ for all } T \in T_h, \mathbf{s}_h = 0 \text{ on } \Gamma^-\}, \tag{24}$$

where Γ^- is the upstream part of Γ. The particle inner product terms in [14] and [16] are discretized using a triangular mesh similar to the one used in [2].

2.3 Collisions and Near-Collisions

When there is more than one particle, the right-hand side of Equation (14) becomes a sum of particle inner product terms, one for each particle, and there is a separate equation like (16) for each particle. If two particles overlap, the problem becomes overconstrained in the overlap region. The two "copies" of Equation (16) represent incompatible side constraints on **u**. And on the right-hand side of Equation (14), the terms corresponding to the two overlapping particles represent two supposedly independent distributed Lagrange multipliers, associated with the respective rigid-body motion constraints. But as just noted, these are constraints are incompatible.

In the finite-element discretized equations, the problem becomes overconstrained even *before* the particles actually overlap. Specifically, it becomes overconstrained when two particles both overlap a single velocity element. The velocity field **u** is a *single* linear function on this element, but the two discretized "copies" of Equation (16) are "trying" to force it to match two different rigid motions (in the portions of the element which overlap the respective particles).

In [1,2], this situation was avoided by imposing a particle-particle repulsive force strong enough to ensure that the particle-particle gap never becomes so small that both particles intersect a single velocity element. In the modified DLM scheme described in this article we allow the particles to touch or slightly overlap, and eliminate the inconsistency in the equations by the following strategy: if each particle inner product is represented by a nonsymmetric matrix, whose rows correspond to the nodes of the particle mesh, and whose columns correspond to the nodes of the velocity mesh, then for a given particle, we "zero out" any column which corresponds to a velocity node which is closer to (the center of) another particle. In other words:

(1) If **v** is a velocity test function corresponding to a given one of the three vertices of a velocity element overlapped by two particles, we drop, from the right-hand side of Equation (14), the particle inner product term corresponding to the particle whose center is farther from the given vertex.

(2) In the "copy" of Equation (16) corresponding to a given particle, if $\boldsymbol{\mu}$ is any particle test function for that particle's mesh and the velocity field **u** is expanded with respect to the global velocity basis functions, then we drop any nonzero terms corresponding to velocity nodes which are closer to another particle.

A little reflection will convince the reader that the resulting equations are no longer overdetermined—even when two particles overlap—as long as the overlap is not too large.

In our code, we impose a repulsive force when the particles overlap. In simulations, the repulsive force is assumed to be large enough so that the overlap between the particles and the walls is smaller than one hundredth of the velocity element size. The additional body force—which is repulsive in nature—is added to equation (8). The particle-particle repulsive force is given by

$$\mathbf{F}_{i,j}^{P} = \begin{cases} 0 & \text{for } d_{i,j} > 2R \\ k(\mathbf{X}_i - \mathbf{X}_j)(2R - d_{i,j}), & \text{for } d_{i,j} < 2R \end{cases} \tag{25}$$

where $d_{i,j}$ is the distance between the centers of the ith and jth particles, R is the particle radius which is assumed to be the same for all particles, $\mathbf{X}_i$ and $\mathbf{X}_j$ are the position vectors of the particle centers, and k is the stiffness parameter. The repulsive force between the particles and the wall is given by

$$\mathbf{F}_{i,j}^{W} = \begin{cases} 0 & \text{for } d_i > 2R \\ k_w(\mathbf{X}_i - \mathbf{X}_j)(2R - d_i), & \text{for } d_i < 2R \end{cases} \tag{26}$$

where d_i is the distance between the centers of the ith particle and the imaginary particle on the other side of the wall Γ_j, and k_w is the stiffness parameter for particle wall collision (see Figure 2). The above particle-particle repulsive forces and the particle-wall repulsive forces are added to equation (8) to obtain

$$M_i \frac{d\mathbf{U}_i}{dt} = M_i\mathbf{g} + \mathbf{F}_i + \mathbf{F}_i'$$

where

$$\mathbf{F}_i' = \sum_{\substack{j=1 \\ j\neq i}}^{N} \mathbf{F}_{i,j}^{P} + \sum_{j=1}^{4} \mathbf{F}_{i,j}^{W} \tag{27}$$

is the repulsive force exerted on the ith particle by the other particles and the walls. The repulsive force acts only when the particles overlap each other.

3. Results

We present the results of several simulations, to demonstrate that the scheme works correctly, and that it reproduces interesting dynamical behavior. According to an analysis by Hesla [3], actual collisions between smooth rigid particles cannot occur in finite time. Hesla gives a rigorous mathematical proof of this fact for Newtonian fluids in both two and three dimensions. He also proves, in the usual case where the "colliding" particles have the same density, that the gap width h(t) between their surfaces will never become smaller than a certain (positive) minimum value h_∞, which depends on the initial conditions of the problem. These results are *exact*—that is, they are obtained directly

from the full Navier-Stokes equations (in conjunction with Newton's equations for the particles), with no approximations of any kind.

Although h(t) will never become zero in the continuous system, it can become exceedingly small in certain situations. In numerical simulations, therefore, numerical truncation errors may allow particles to actually touch, or even overlap.

3.1. Sedimentation

We next discuss the numerical results obtained using the above algorithm for the particle-particle interactions. The particles are suspended in Newtonian and Oldroyd-B fluids. The parameter c in the Oldroyd-B model will be assumed to be 7, i.e., $\eta_p = 7\ \eta_s$. The parameter in the particle-particle and particle-wall force models k and k_w are equal to 10^4 which was picked to ensure that the particles do not overlap more than a one hundredth of the velocity element size. We will also assume that all dimensional quantities are in the CGS units.

3.1.1. Newtonian Fluid

We begin by investigating the case of two circular particles sedimenting in a channel filled with a Newtonian fluid. One of the objectives of this study is to show that the particle trajectories before collision are independent of the mesh resolution and the time step. We have used two regular triangular meshes to show that the results converge with mesh refinement. In a triangular element there are six velocity and three pressure nodes, and thus the size of the velocity elements is one half of that of the pressure elements. The particle domain is also discretized using a triangular mesh similar to the one used in [2]. The size of velocity elements for the first mesh is 1/96, and for the second mesh is 1/144. The size of particle elements for the first mesh is 1/70, and for the second mesh is 1/125. The number of velocity nodes and elements in the first mesh are 111361 and 55296, respectively. In the second mesh, there are 249985 velocity nodes and 124416 elements. The time step for these simulations is 0.001 or 0.0004.

For these calculations $\eta = 0.08$ and $\rho_L = 1.0$, and the particle diameter and density are 0.2 and 1.1, respectively. The initial velocity distribution in the fluid, and the particle velocities are:

$$\mathbf{u}_0 = 0,$$

$$\mathbf{U}_{10} = \mathbf{U}_{20} = 0\,,$$

$$\omega_{10} = \omega_{10} = 0\,.$$

The channel width is 2 and height is 6. The simulations are started at t=0 by dropping two particles at the center of the channel at y= 5.0 and 5.3.

It is well known that when two particles are dropped close to each other in a Newtonian fluid they interact by undergoing repeated drafting, kissing and tumbling [9,10]. From Figure 3 and 4 we note that initially both particles accelerate downwards until they reach the terminal velocity at $t \approx 0.4$. From these figures we also note that the particle in the wake falls more rapidly than the particle in front, as the drag acting on it is smaller. Thus, the gap between them decreases with time and they touch or kiss each other at t=~0.4 (see Figure 5). After touching each other, the particles fall together with an approximately constant velocity of ~ 4.0. The Reynolds number based on this velocity is ~10. The maximum overlap between the particle is less than 0.00007, which is approximately one hundredth of the velocity element size. Also notice that when the upper particle touches the lower particle the y-components of their velocities become approximately equal until they tumble and subsequently separate from each other. The tumbling of particles takes place because the configuration where they are aligned parallel to the flow direction is unstable (see Figure 5c).

The velocity distribution around sedimenting particles is shown in Figure 5a-c. In Figure 5a the two particles are aligned approximately parallel to the sedimentation direction. The particles are touching each other. Figure 5b shows the velocity distribution at t=0.625 when the particles are beginning to tumble. The last figure in the sequence shows the velocity distribution when the particles have separated from each other. These figures show that the velocity at the nodes that are closer to the upper particle is constrained by the upper particle, and that for the nodes closer to the lower particle is constrained by the lower particle. The method therefore allows the particles to touch as well as slightly overlap each other.

In Figures 3 and 4 we have shown the x and y-components of positions and velocities as a function of time for the two meshes described above using the time steps of 0.001 and 0.0004. From Figure 3 we note that when the number of nodes used is approximately doubled the x- and y-components of velocities and positions for both particles (marked 1 and 2) before collision, i.e., for $t<0.4$, remain approximately the same. The results obtained for the finer mesh are denoted by 1' and 2'. Similarly, a comparison of the curves marked (1 and 1') and (2 and 2') in Figure 4 shows that when the time step is reduced by a factor of 2.5 the temporal evolutions of the particle velocities and trajectories do not change significantly which shows that the results for $t<0.4$ are also independent of the time step. The motion of particles for $t>0.4$ is influenced by the particle-particle collision and the instability that makes the alignment of particles parallel to the flow direction unstable. The trajectories for $t>0.4$ are therefore sensitive to the mesh size and the time step. We may therefore conclude that for $t<0.4$—the time duration for which the particle-particle interactions do not significantly influence the motion of the particles—the results are independent of the mesh resolution.

3.1.2. Oldroyd-B Fluid

When two particles sediment in a channel filled with a viscoelastic liquid the stable configuration is the one where the particles are aligned parallel to the flow direction. For these simulations the channel width is 2 and height is 6. The velocity element size is 1/96, and the size of the particle elements is 1/70. The fluid density is 1.0, and the particle density is 1.07. The fluid viscosity is 0.24 and relaxation time is 0.3, and the particle diameter is 0.2. The time step used for all results reported this subsection is 0.0001.

In Figures 6a and b, the positions of the two particles and tr**A** distributions for t=1.0 and 3.0 are shown. The particles were dropped at a distance of 0.15D from each other at t=0. The Reynolds number of the particles is 0.48 and De=1.725. Also note that since the velocity of the particle on the top is larger, the distance between them decreases with time. The distance decreases to approximately 0.0001D at t=1.0. From Figure 6a-b, where we have shown the isovalues of tr**A**, we note that tr**A** in front of the leading particle and around the particles is relatively large. This figure also shows that it takes some time for the fluid to relax back to the state of equilibrium. This gives rise to the characteristic streak lines that are indicative of the hyperbolic nature of the constitutive equation for the stress. For this case since the Mach number is 0.9 and the elasticity number is 3.59, there is a strong tendency for the particles to align parallel to the falling direction. The velocity distribution around particles is shown in Figure 6c.

When more than two particles sediment in a viscoelastic liquid the stable configuration is the one where they are aligned parallel to the sedimentation direction. To simulate this, we consider sedimentation of ten particles in a channel of width 2 and height 8. The fluid density is 1.0, and the particle density is 1.07. The fluid viscosity is 0.24 and relaxation time is 0.3, and the particle diameter is 0.2. The velocity element size is 1/96, and the size of the particle elements is 1/70. The simulations are started at t=0 by placing the particles in a vertical arrangement along the channel center. The distance between the particles is 1.5D and the center of the first particle is at 5.0. The particles are dropped with zero linear and angular velocities, and the fluid is in the quiescent relaxed state. The average Deborah number is 1.73, the average Reynolds number is 0.5, the Mach number is 0.93 and the elasticity number is 3.46. The distribution of tr**A** and the particle positions at t=0.88 is shown in Figure 7. We note that the particles are aligned approximately parallel to the sedimentation direction and the distance between the particles of the chain is very small. In fact, some of the particles are slightly overlapping each other. The repulsive body force is needed to ensure that the overlap is sufficiently small.

3.2. Time Evolution of Gap Width in Newtonian Fluids

In situations in which the lubrication force dominates all other contributions to the total hydrodynamic force, the equations of motion of the particles can be solved explicitly, yielding explicit formulas for the time evolution of the gap width h(t), as shown by Hesla [3]. These formulas apply to the "collision" between a free particle and a (stationary) rigid bounding wall, as well as to the "collision" between two free particles, the wall acting as a large, funny-shaped particle constrained to remain motionless.

In this section we compare Hesla's formula for h(t) with the DLM results for collisions between a particle and a wall, as well as for collisions between two particles. The domain used in these calculations is square shaped with sides 20 R. The velocity element size is 1/240, and the size of the particle elements is 1/230. The fluid viscosity is varied. The fluid density is 1.0. The particle density is varied and its radius is 0.1. The initial fluid velocity in the domain is assumed to be zero and the time step is 0.0001.

3.2.1. Gravity-Driven "Collision"

For a gravity-driven "collision," the gap width h(t) must continue to decrease indefinitely. For example, when a negatively buoyant free circular particle sediments toward a stationary flat wall in two dimensions, Hesla shows that (when the lubrication force is dominant) for large t,

$$\frac{1}{h(t)^{1/2}} = \frac{(M-m)gt}{2C} + C1 + o(1) \qquad (28)$$

where C is a constant, M is the mass of the particle, m is the mass of the displaced fluid, g is the acceleration of gravity, and C1 is a constant that depends on the initial conditions. The constant C depends on the fluid viscosity and the particle radius. Its exact value must be determined using the method of asymptotic analysis.

In Figure 8a we have plotted $\frac{1}{h(t)^{1/2}}$ as a function of time for two different values of the particle density for the case where particle sediments under gravity over a fixed wall, and in Figure 8b similar results are shown for the case of two particles. In the two particle case the lower particle is assumed to be fixed and the upper particles sediments under gravity. The fluid properties are kept fixed and the initial particle velocity is assumed to be zero.

From these two figures we note that $\frac{1}{h(t)^{1/2}}$ increases with time but the curvature decreases with time. Also note that for the curves marked 1 for t>~0.7 in Figure 8a and for t>~2.1 in Figure 8b

$\frac{1}{h(t)^{1/2}}$ increases linearly with time, as suggested by expression (28). The curves marked 2 also show a similar linear behavior. These results show that simulations correctly capture the asymptotic behavior of a particle sedimenting onto a horizontal wall or another fixed particle. In Figure 8a where the particle approaches a wall $\frac{1}{h(t)^{1/2}}$ curve becomes approximately horizontal when the distance between the particle and the wall is approximately equal to the size of one velocity element, indicating that in simulations the particle decelerates faster than that is given by asymptotic analysis. This sudden decrease in the particle velocity is due to the discrete incompressibility constraint. In Figure 8b however the particle deceleration is relatively slower and the particle distance from the wall becomes much smaller than the size of one velocity element.

3.2.2. Non-Driven "Collision"

For cases where there is no net buoyancy force difference driving the "collision", Hesla shows that the gap width h(t) between the two surfaces will never become smaller than a certain (positive) minimum value h_∞, which depends on the initial conditions of the problem. For example, when a neutrally buoyant free circular particle is "thrown" toward a stationary flat wall in two dimensions, Hesla shows that (when the lubrication force is dominant)

$$\frac{1}{h_\infty^{1/2}} \approx \frac{1}{h_0^{1/2}} + \frac{MU_0}{2C} \tag{30}$$

where $h_0=h(0)$ and U_0 is the magnitude of the initial velocity, and that for large t,

$$\log\left(\frac{h}{h_\infty} - 1\right) = -\frac{C}{Mh_\infty^{3/2}} t \quad + C2 + o(1) \tag{31}$$

where C2 depends on the initial conditions.

For a fixed value of h_0, in Figure 9a we have plotted $\frac{1}{h_\infty^{1/2}}$ as a function of U_0 for the case where a particle approaches a wall and in Figure 9b for the case where a particle approaches a fixed particle of the same size. The value h_0 for all cases in Figure 9a is 4R and in Figure 9b is R. From these figures we note that, as expected, $\frac{1}{h_\infty^{1/2}}$ increases when initial particle velocity is increased and $\frac{1}{h_\infty^{1/2}}$

varies linearly with U_0, as suggested by Hesla's analysis. In both figures for the last point the value of h_∞ is less than the size of the velocity element, and thus the truncation errors are of the same order as h.

In Figure 10a we have plotted $\log(\frac{h}{h_\infty}-1)$ as a function of t for the case where a particle approaches a wall, for four different values of U_0, and in Figure 10b for the case where a particle approaches a fixed particles of the same size head on. In these calculations the initial fluid velocity is assumed to be zero and only the initial particle velocity is varied. In Figure 10a for all four cases and in Figure 10b for the three cases, $\log(\frac{h}{h_\infty}-1)$ varies linearly with time as $h \to h_\infty$, as suggested by expression (31). From (31) we note that the slope in the linear region is $-\alpha$. Our simulations, therefore, correctly capture the asymptotic particle motion as well as the role of lubrication forces as the particle approaches the wall.

4. Conclusions

The modified DLM method developed in this paper allows particles to come arbitrarily close to each other, including slightly overlap each other. When conflicting rigid body motion constraints from two different particles are applicable on a velocity node, the constraint from the particle that is closer to the node is used and the other constraint is dropped. A repulsive force is applied when the particles overlap each other to limit the overlap. In our simulations, the particles are allowed to overlap as much as 1/100 of the velocity element size. The modified distributed Lagrange multiplier/fictitious domain method could be used to study the particle-particle interactions as well as the collisions between particles suspended in the Newtonian and Oldroyd-B fluids.

In order to validate our code we have simulated the time dependent interactions between two particles sedimenting in Newtonian and Oldroyd-B fluids. We have verified that the results are independent of the mesh resolution as well as the size of time step. Our simulations show that when particles are dropped in a channel, and the viscoelastic Mach number (M) is less than one and the elasticity number (E) is greater than one, the particles form a chain parallel to the flow direction and the particles in the chain touch each other. The particles dropped in a Newtonian liquid undergo characteristic drafting, kissing and tumbling. The particles touch each other during the kissing phase. Our results for the time dependent motion of a particle moving towards a wall are in agreement with the asymptotic analytical results for a particle thrown with a fixed velocity towards the wall and also for the case of a particle sedimenting on a horizontal surface.

Acknowledgements

This work was partially supported by National Science Foundation KDI Grand Challenge grant (NSF/CTS-98-73236), the Department of Basic Energy Science at DOE and the University of Minnesota Supercomputing Institute.

5. References

[1] R. Glowinski, T.W. Pan, T.I Hesla and D.D. Joseph, A distributed Lagrange multiplier/fictitious domain method for particulate flows. Int. J. of Multiphase Flows. **25** (1998), 755-794.

[2] P. Singh, D.D. Joseph, T.I Hesla, R. Glowinski and T.W. Pan, Direct numerical simulation of viscoelastic particulate flows, *J. of Non Newtonian Fluid Mechanics* 91, 165-188 (2000).

[3] T.I. Hesla, No collisions in viscous fluids!, in preparation (2001).

[4] P.Y. Huang, H.H. Hu and D.D. Joseph, Direct simulation of the sedimentation of elliptic particles in Oldroyd-B fluids, *J. Fluid Mech*. **362** (1998), 297-325.

[5] H.H. Hu Direct simulation of flows of solid-liquid mixtures. *Int. J. Multiphase Flow*, **22** (1996), 335-352.

[6] P.Y. Huang, J. Feng, H.H. Hu and D.D. Joseph, Direct simulation of the motion of solid particles in Couette and Poiseuille flows of viscoelastic fluids, *J. Fluid Mech*. **343** (1997), 73-94.

[7] R. Glowinski, T.W. Pan and J. Periaux, A Lagrange multiplier/fictitious domain method for the numerical simulation of incompressible viscous flow around moving rigid bodies, *C.R. Acad. Sci. Paris* **324** (1997), 361-369.

[8] V. Girault, R. Glowinski and T.-W. Pan, A fictitious domain method with distributed multiplier for the Stokes problem, Applied nonlinear analysis, Kluwer Academic/Plenum Publisher, 1999, 159-174.

[9] A. Fortes, D.D. Joseph and T. Lundgren, Nonlinear mechanics of fluidization of beds of spherical particles, *J. Fluid Mech.* **177** (1987),497-483.

[10] D.D. Joseph, A. Fortes, T. Lundgren and P. Singh, Nonlinear mechanics of fluidization of beds of spheres, cylinders, and disks in water, *Advances in Multiphase Flow and Related Problems (Edited by Papanicolau, G.)* **16** (1987), 35-42.

6. Figures

Figure 1. A typical rectangular domain used in our simulations; Γ^- is the upstream portion of Γ .

Figure 2. The imaginary particle used for computing the repulsive force acting between a particle and a wall.

Figure 3. The velocity components u and v and the positions x and y of the sedimenting circles are shown as a function of time. The size of the velocity elements is 1/96, and the size of the particle elements is 1/70. The time step for the curves marked 1 and 2 is 0.001 and for the curves marked 1' and 2' is 0.0004.

Figure 4. The velocity components u and v and positions x and y of the sedimenting circles are shown as a function of time. For curves marked 1 and 2 the size of the velocity elements is 1/96 and the size of the particle elements is 1/70 and for the curves marked 1' and 2' the size of the velocity elements is 1/144, and the size of the particle elements is 1/125. The time step is 0.0004.

Figure 5. The size of the velocity elements is 1/96, and the size of the particle elements is 1/70. The time step is 0.0004. The velocity fields at t=0.5, 0.625 and 0.878 are shown in (a), (b) and (c), respectively.

Figure 6. The size of the velocity elements is 1/96, and the size of the particle elements is 1/70. The time step is 0.0004. The two particles are dropped at t=0 at y=5.0 and y=5.3 along the channel center. (a) Isovalues of tr**A** at t=1.0, (b) Isovalues of tr**A** at t=3.0, (c) The velocity field at t=1.0.

Figure 7. Isovalues of tr**A** at t=1.1 for ten particles sedimenting in a channel filled with Oldroyd-B fluid is shown. The parameters are the same as in Figure 6.

Figure 8. $\frac{1}{h(t)^{1/2}}$ is plotted as a function of time. The circle is released from a state of rest. (a) Circle sediments onto a fixed wall. The particle density for the curve marked 1 is 1.02 and for 2 is 1.05. The fluid viscosity is 0.08 and h_0=3R. (b) Circle sediments onto a fixed circle of the same diameter. The particle density for the curve marked 1 is 1.02 and for 2 is 1.1. The fluid viscosity is 2.0 and h_0=0.7R.

Figure 9. The asymptotic distance $\frac{1}{h_\infty^{1/2}}$ is plotted as a function of the initial particle velocity. (a) Circle is thrown towards a fixed wall. The particle density is 5.0 and the fluid viscosity is 0.2. (b) Circle is thrown towards another fixed circle of the same diameter. The particle density is 5.0 and the fluid viscosity is 0.8.

Figure 10. $\log(\frac{h}{h_\infty} - 1)$ is plotted as a function of time for several different values of the initial velocity. The parameters are the same as in Figure 9. (a) Circle is thrown towards a fixed wall. (b) Circle is thrown towards another fixed circle of the same diameter.

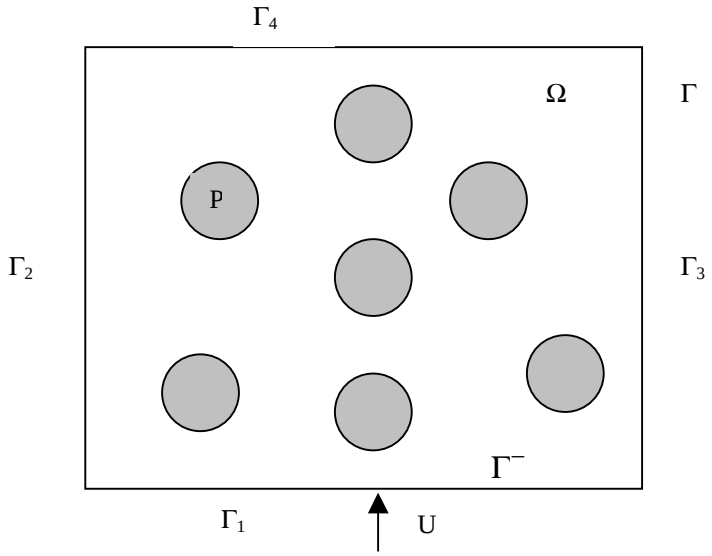

Figure 1.

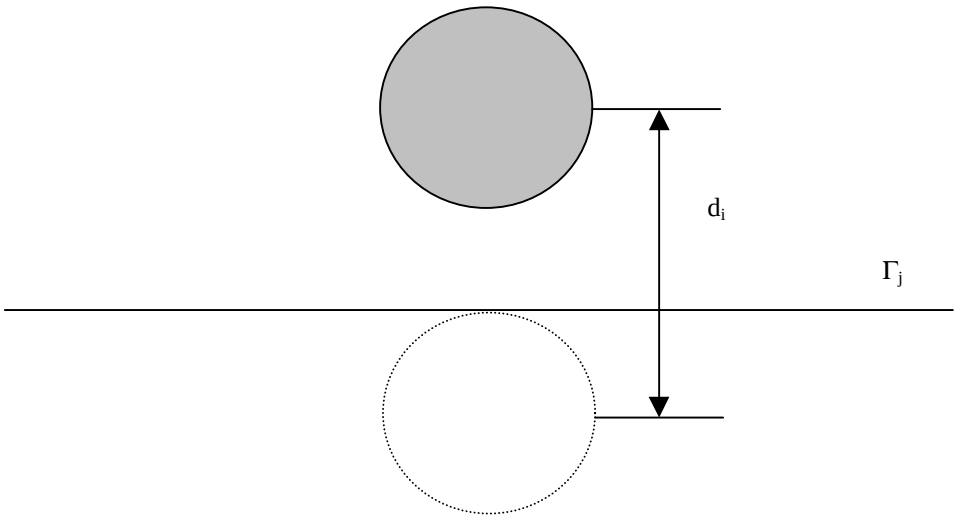

Figure 2

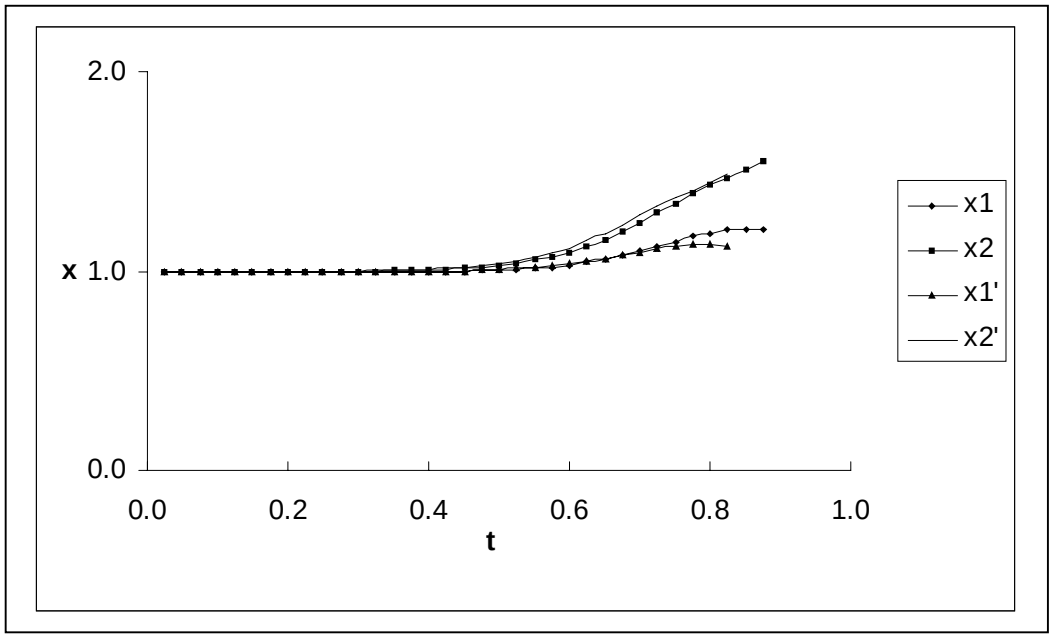
2.0
x 1.0
0.0
0.0
0.2
0.4
0.6
0.8
1.0
t
x1
x2
x1'
x2'

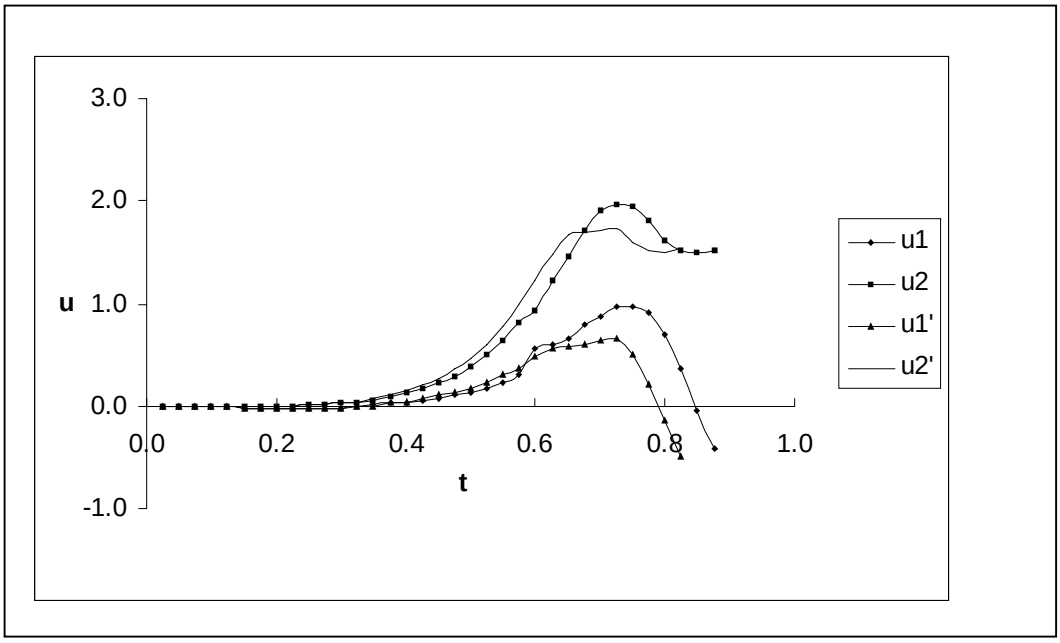
3.0
2.0
u 1.0
0.0
-1.0
0.0
0.2
0.4
0.6
0.8
1.0
t
u1
u2
u1'
u2'

Figure 3a-b

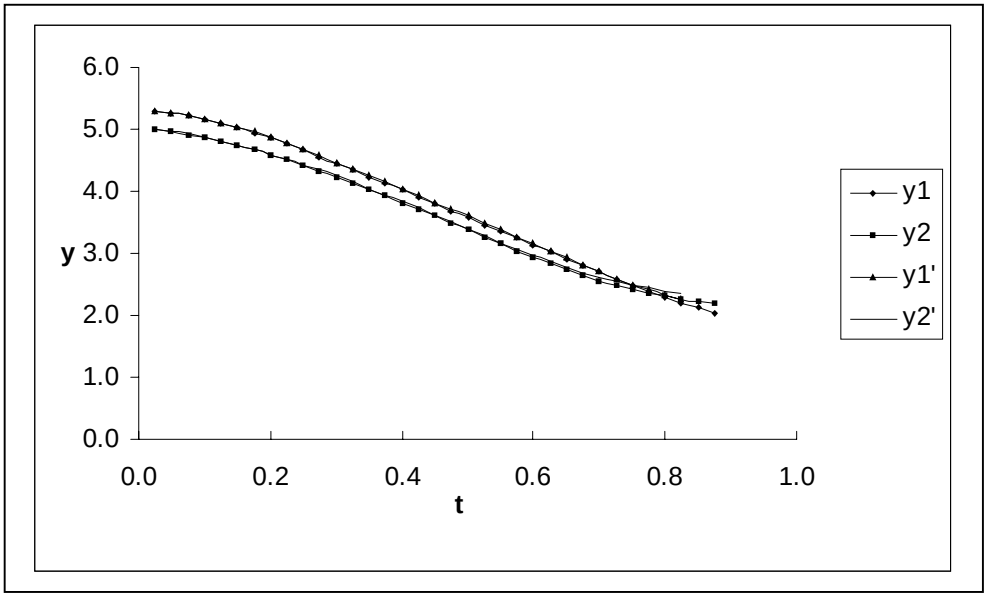
6.0
5.0
4.0
y 3.0
2.0
1.0
0.0
0.0
0.2
0.4
0.6
0.8
1.0
t
y1
y2
y1'
y2'

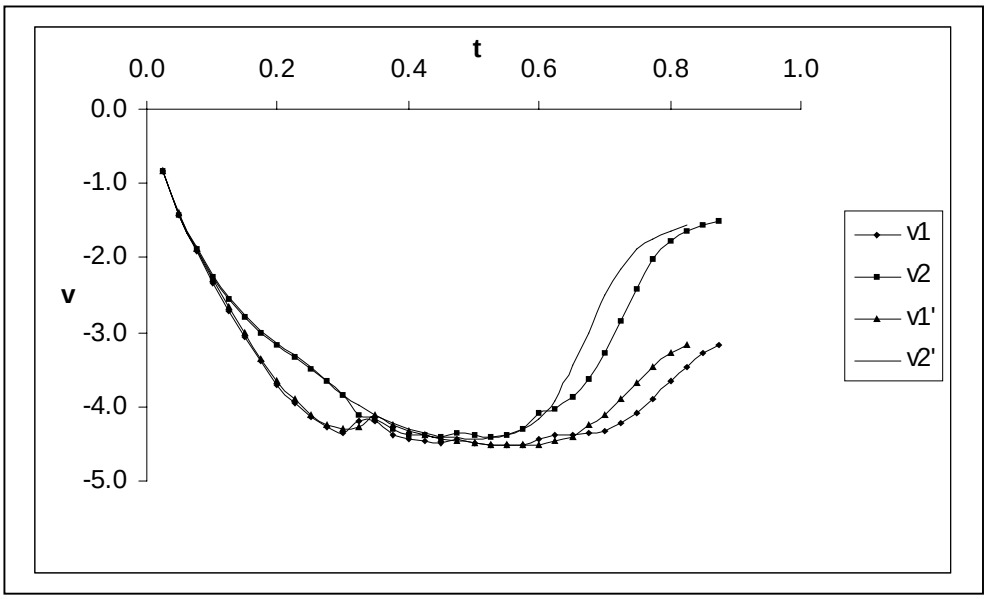
t
0.0
0.2
0.4
0.6
0.8
1.0
0.0
-1.0
-2.0
v
-3.0
-4.0
-5.0
v1
v2
v1'
v2'

Figure 3c-d

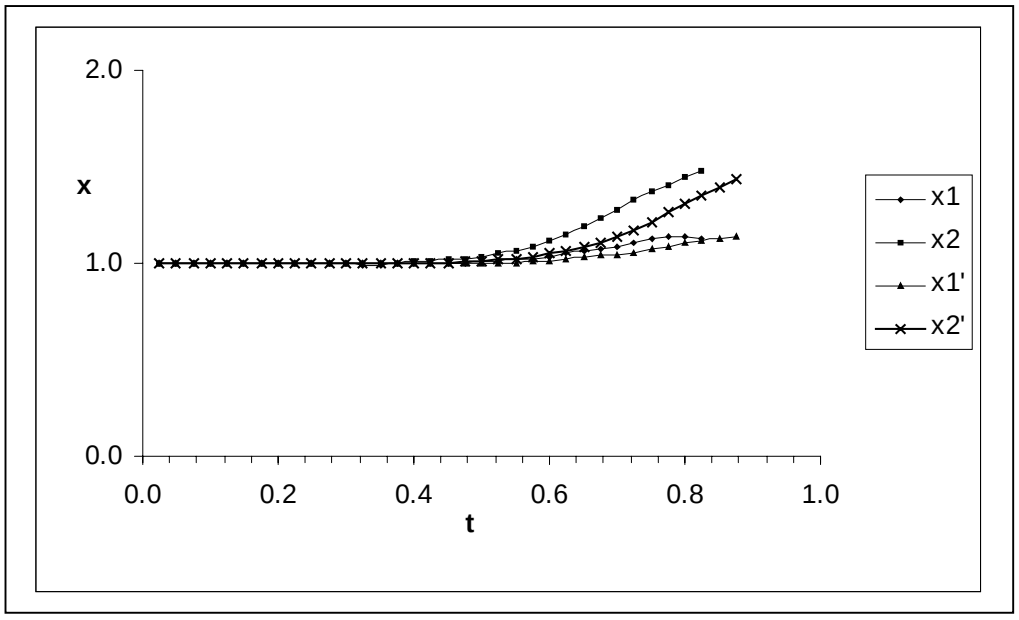
2.0
x
1.0
0.0
0.0
0.2
0.4
0.6
0.8
1.0
t
x1
x2
x1'
x2'

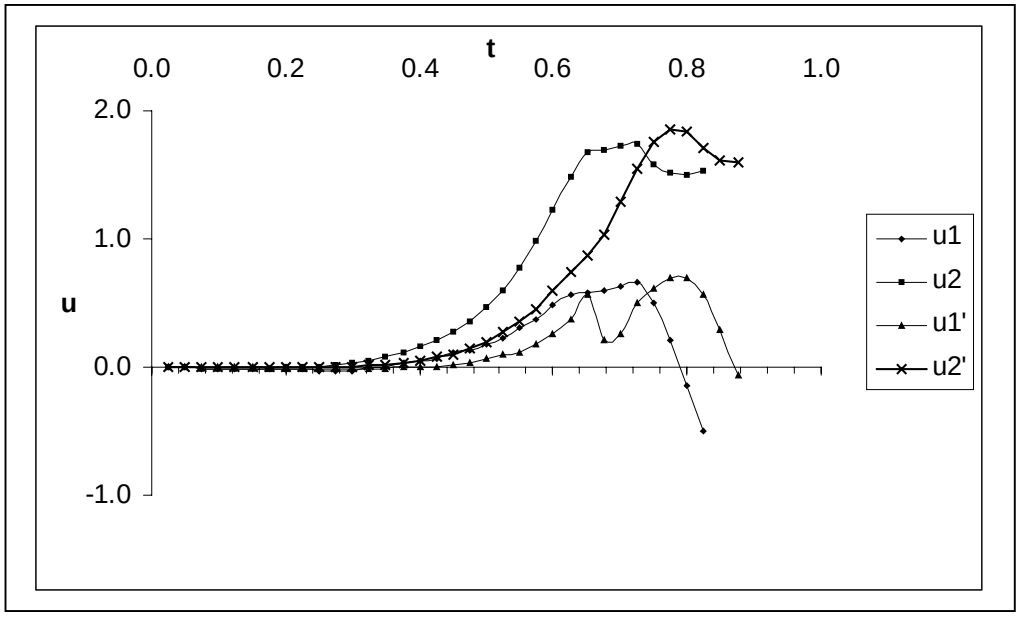
t
0.0
0.2
0.4
0.6
0.8
1.0
2.0
1.0
u
0.0
-1.0
u1
u2
u1'
u2'

Figure 4a-b

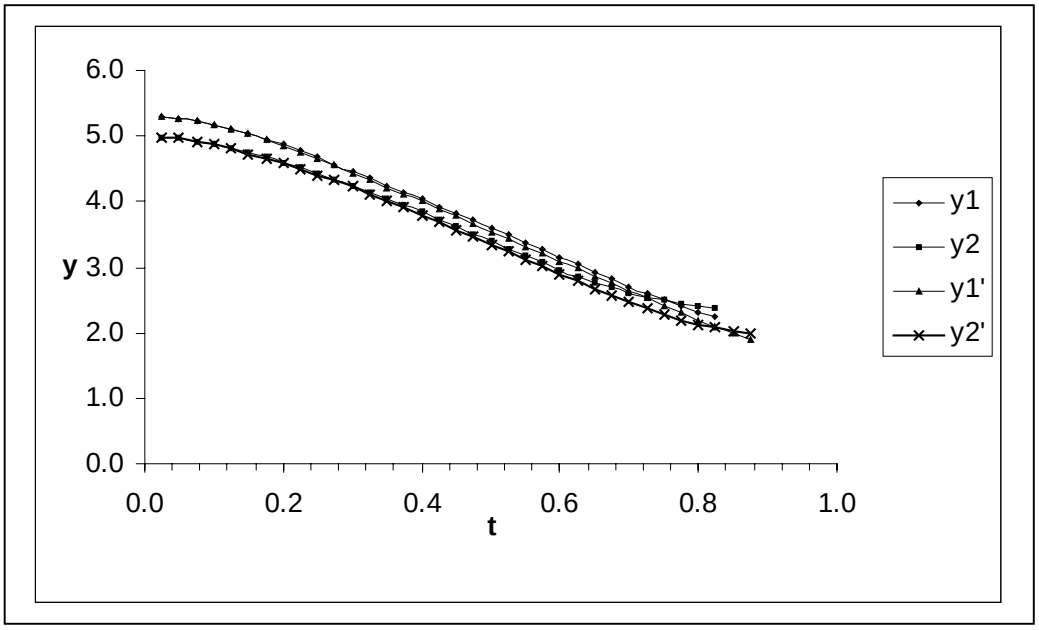
6.0
5.0
4.0
y 3.0
2.0
1.0
0.0
0.0
0.2
0.4
0.6
0.8
1.0
t
y1
y2
y1'
y2'

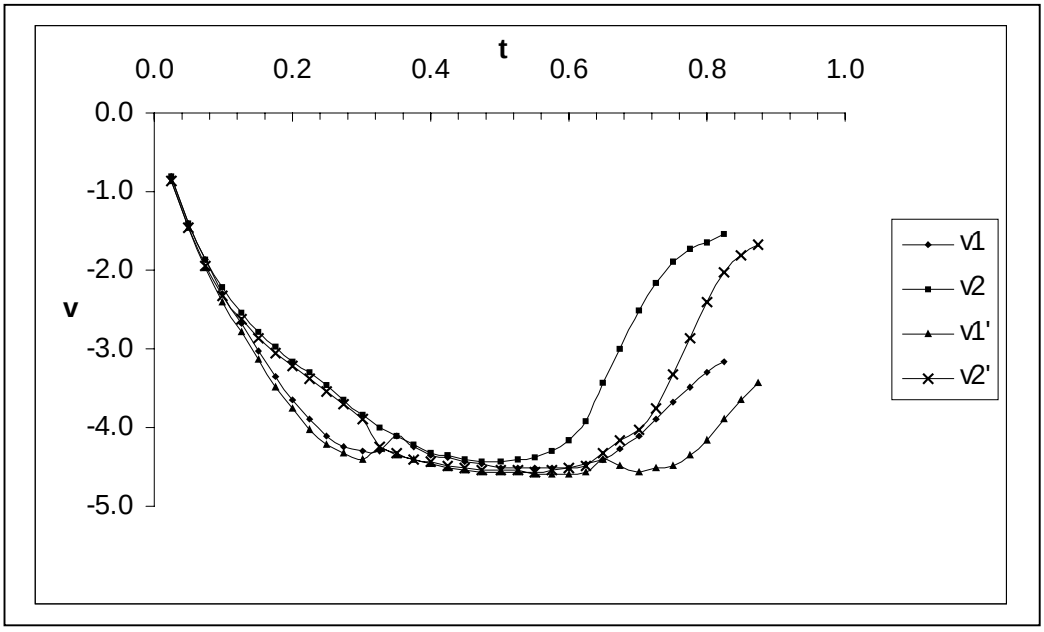
t
0.0
0.2
0.4
0.6
0.8
1.0
0.0
-1.0
-2.0
v
-3.0
-4.0
-5.0
v1
v2
v1'
v2'

Figure 4c-d

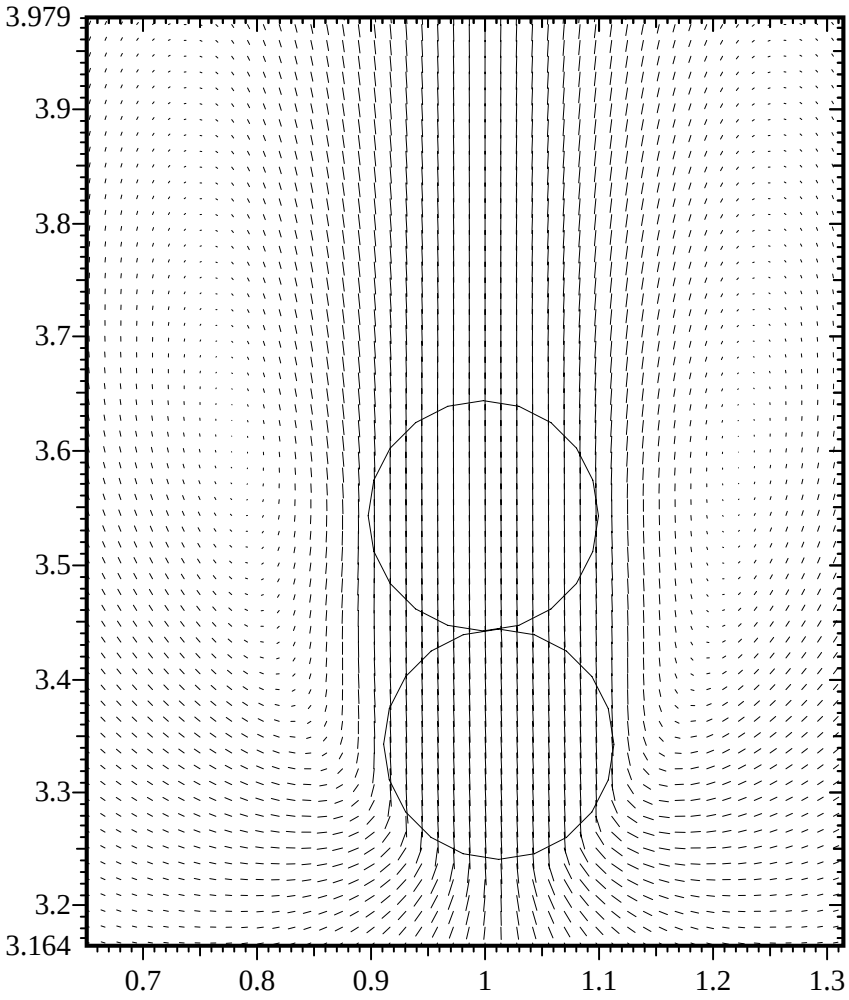

Figure 5a.

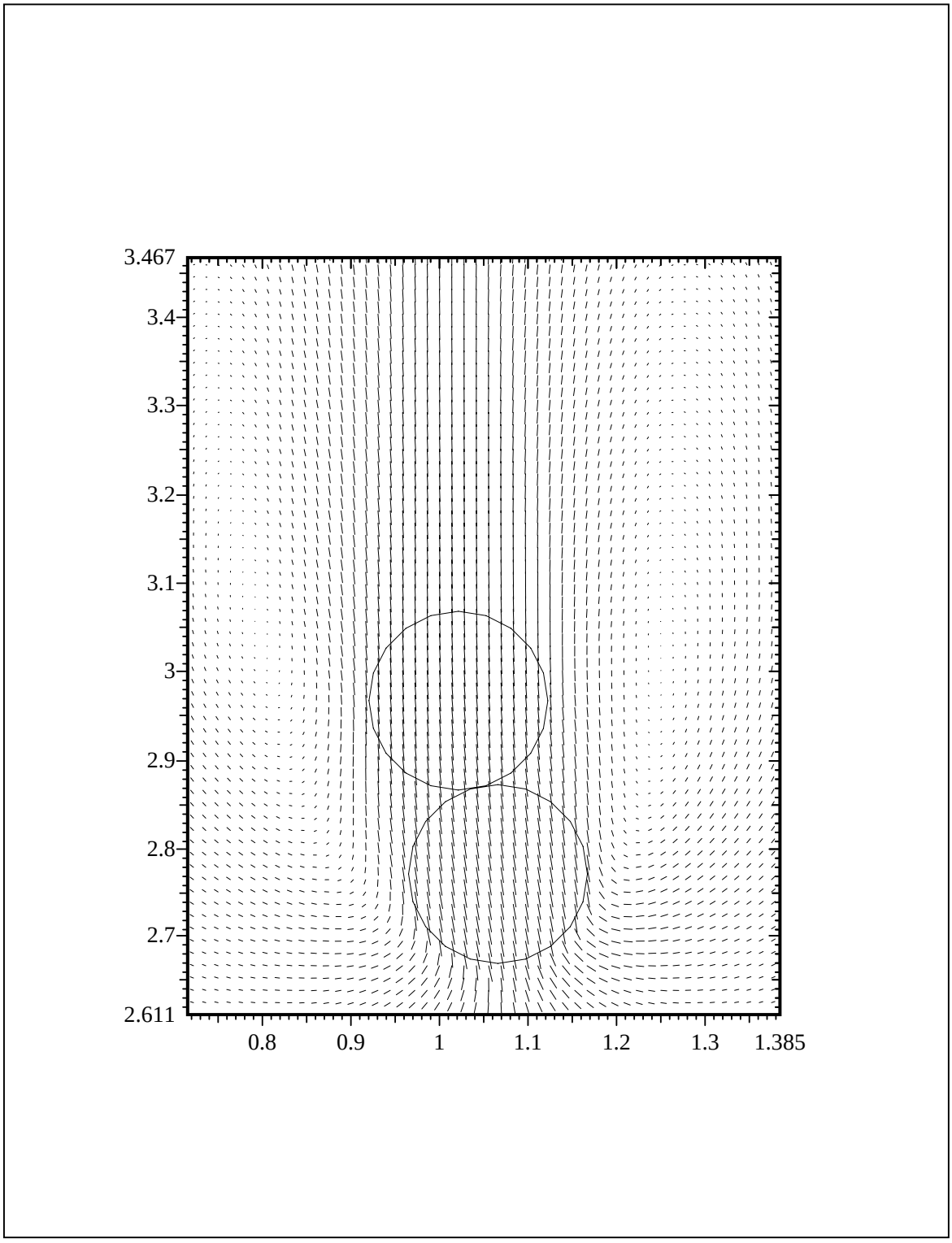

Figure 5b.

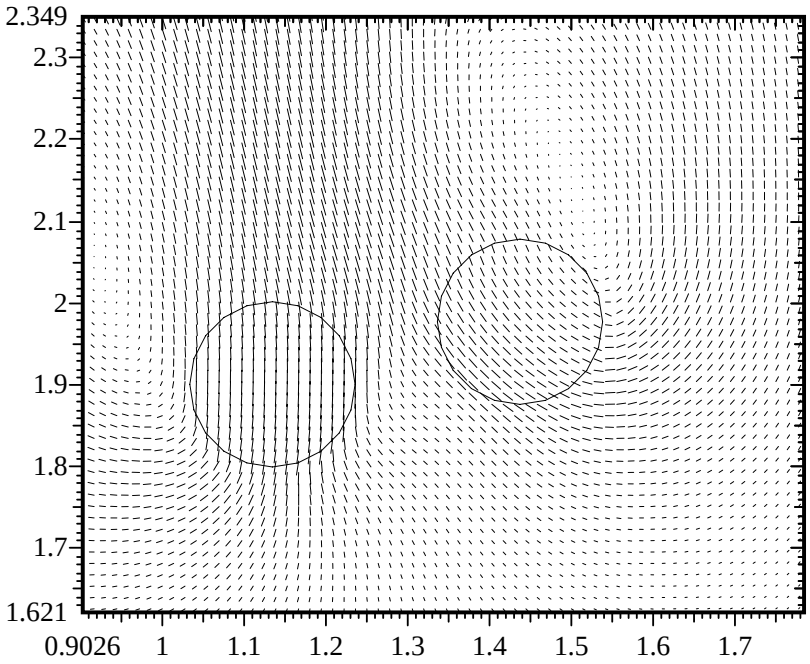

Figure 5c.

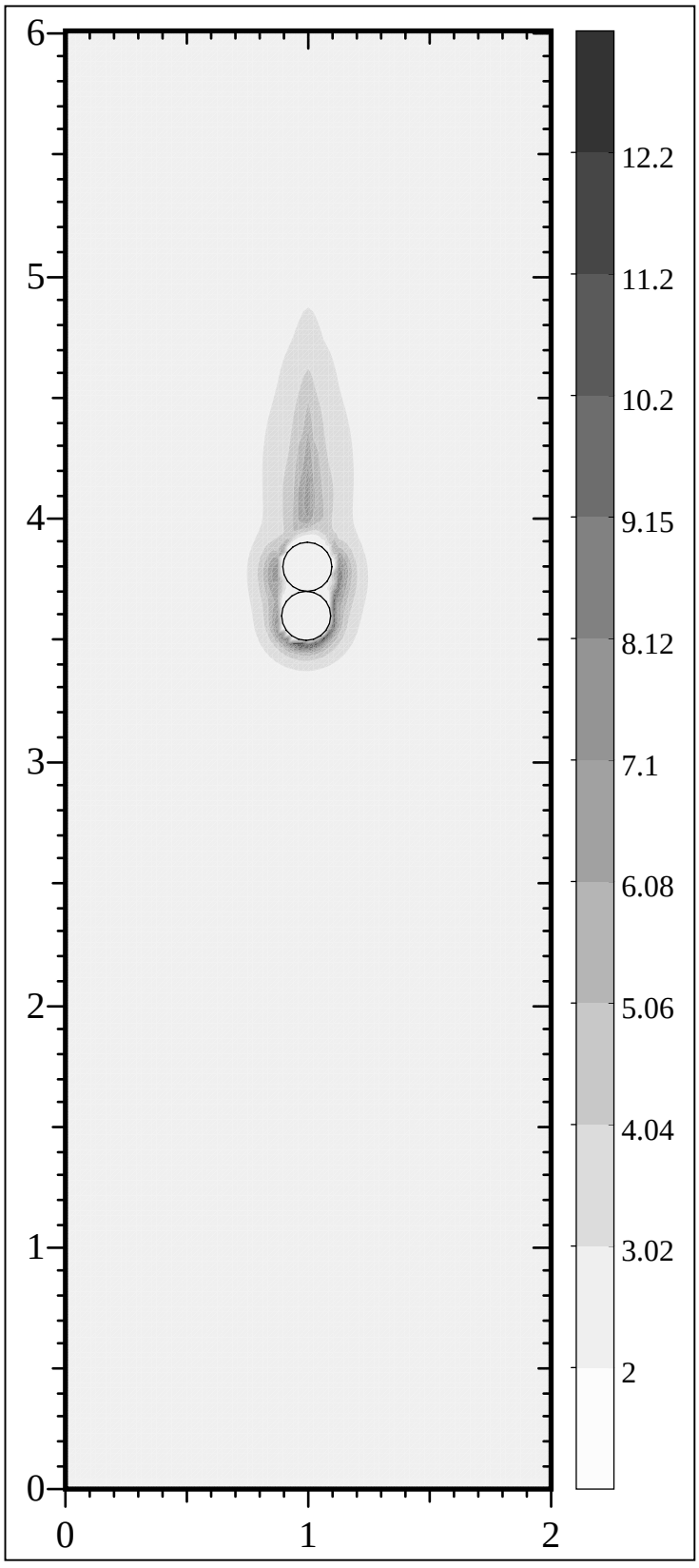

Figure 6a.

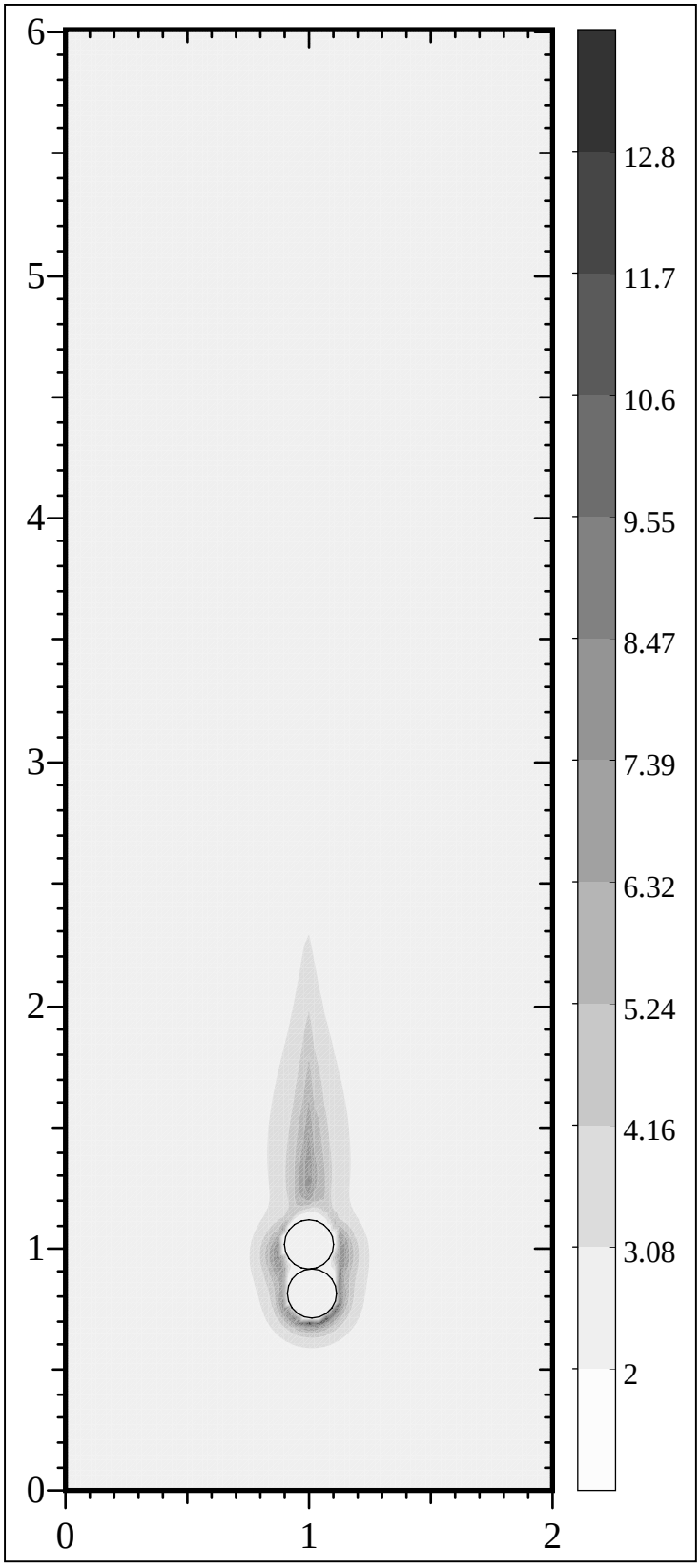

Figure 6b.

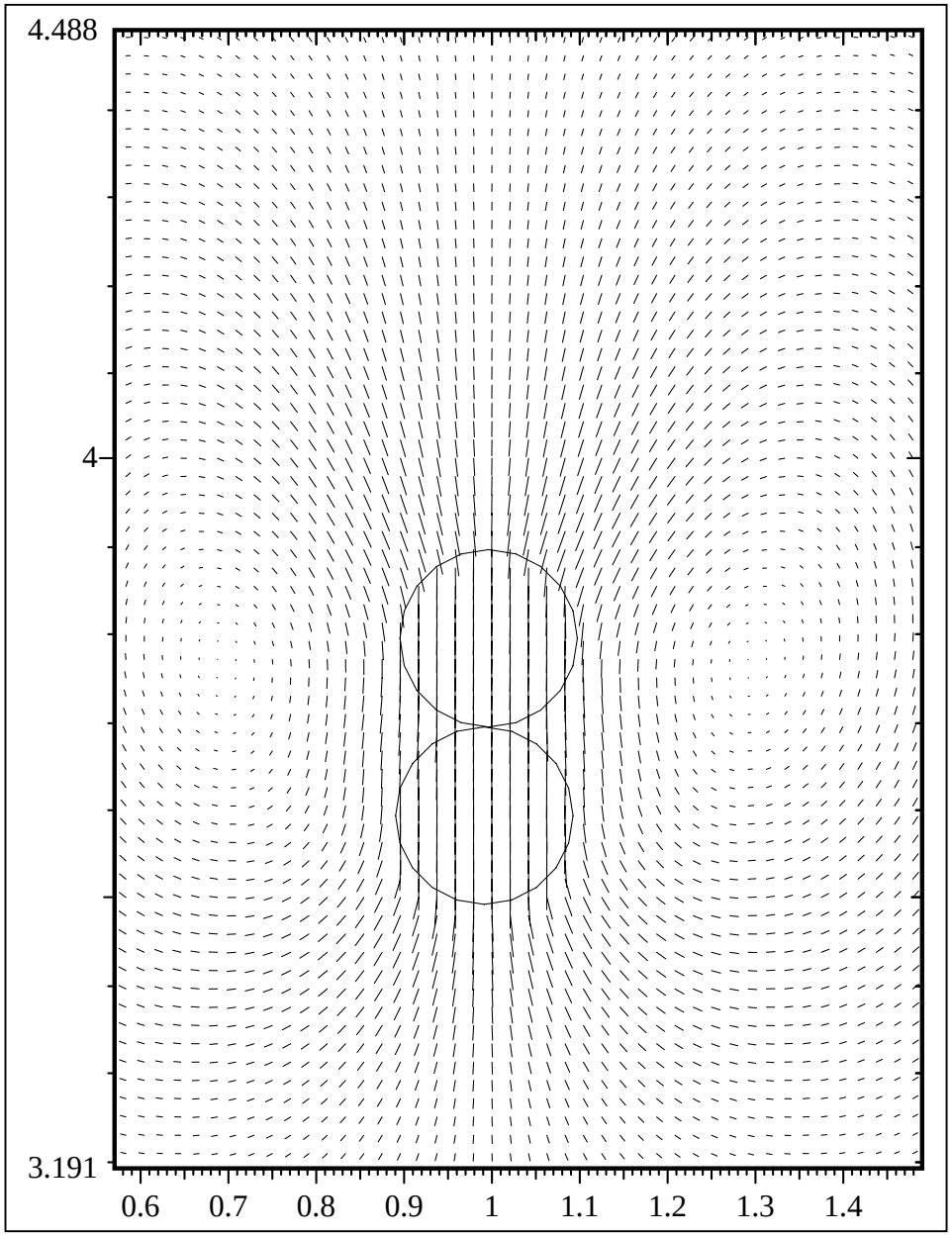

Figure 6c.

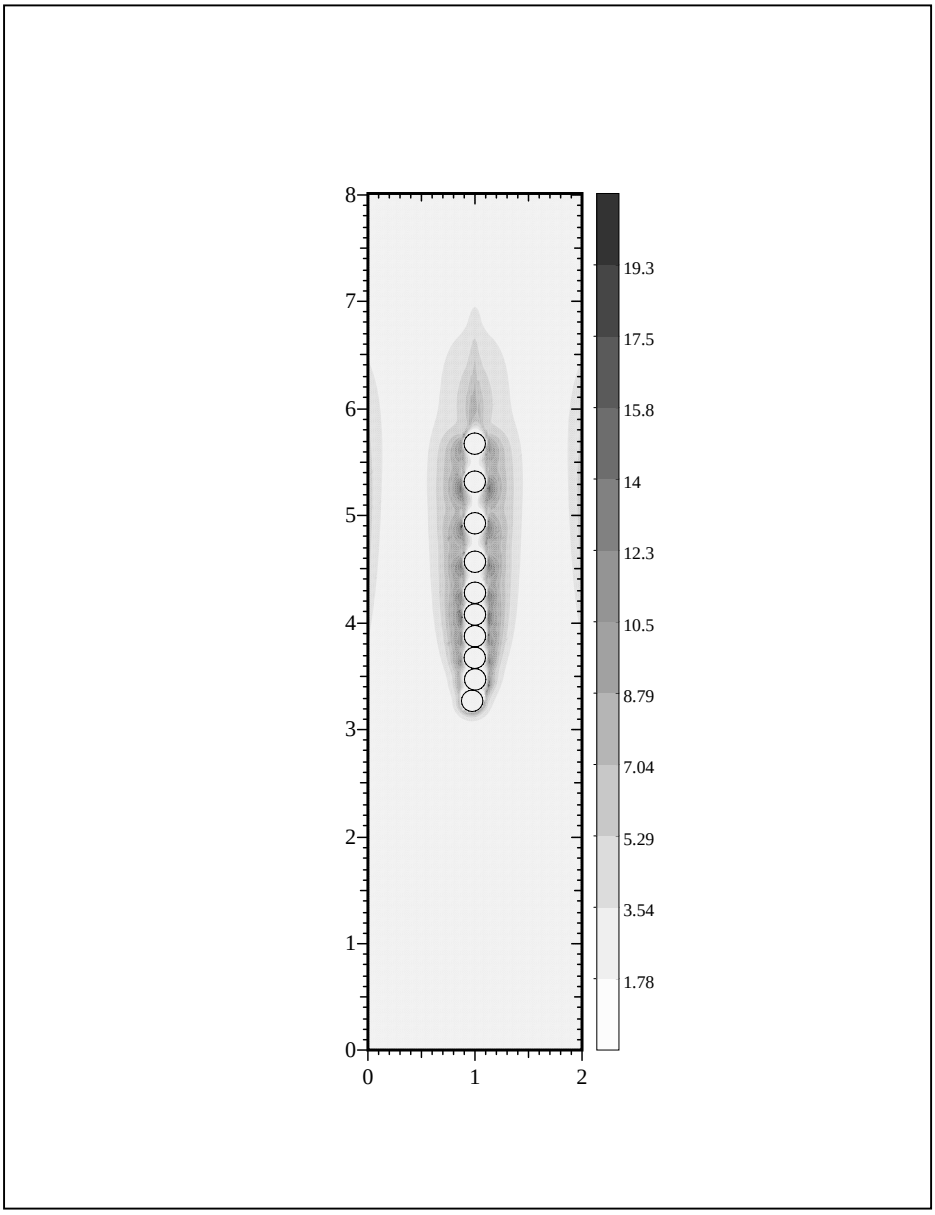

Figure 7.

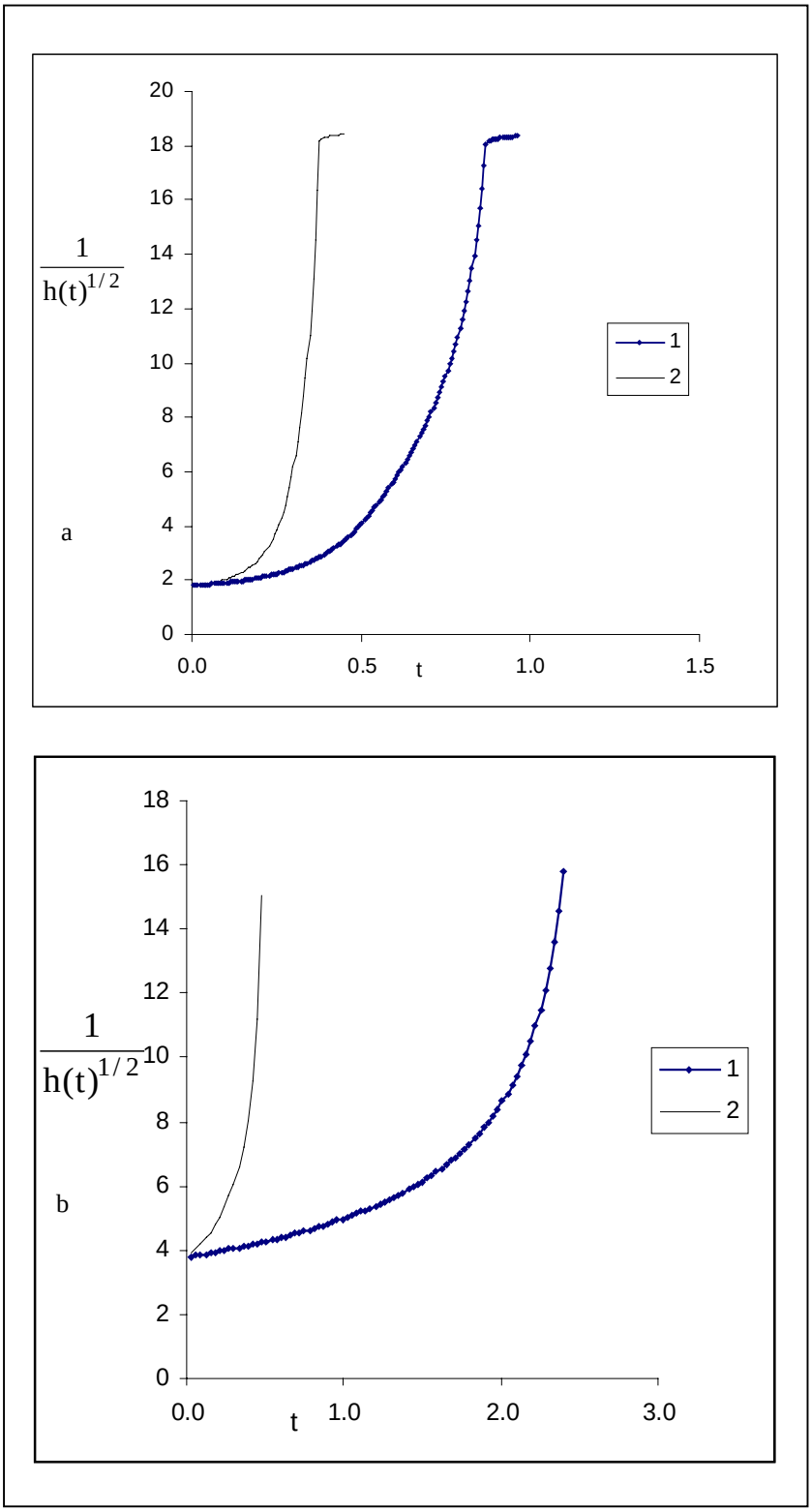

Figure 8. (a) and (b).

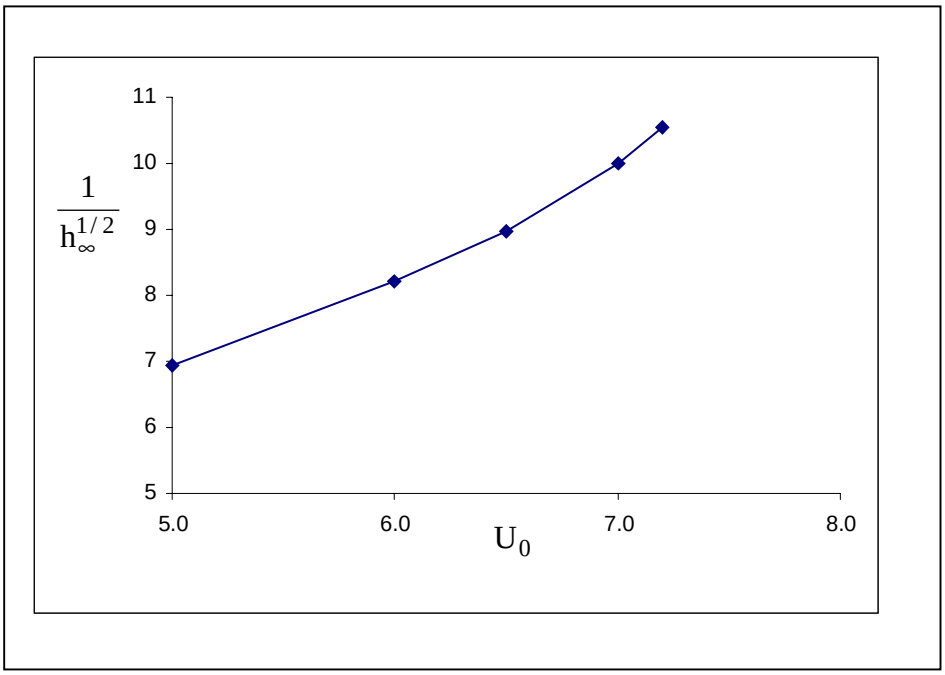

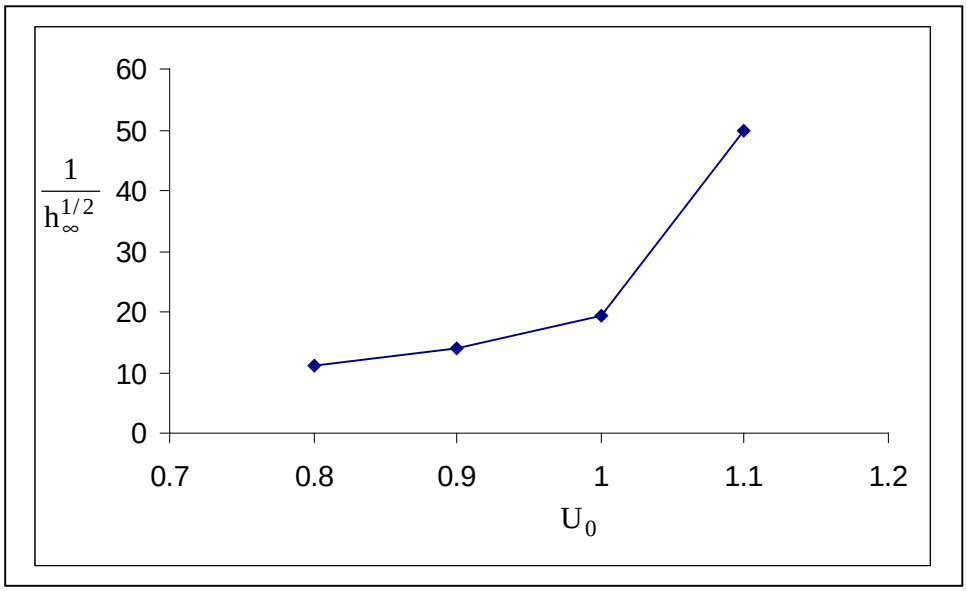

Figure 9 a and b.

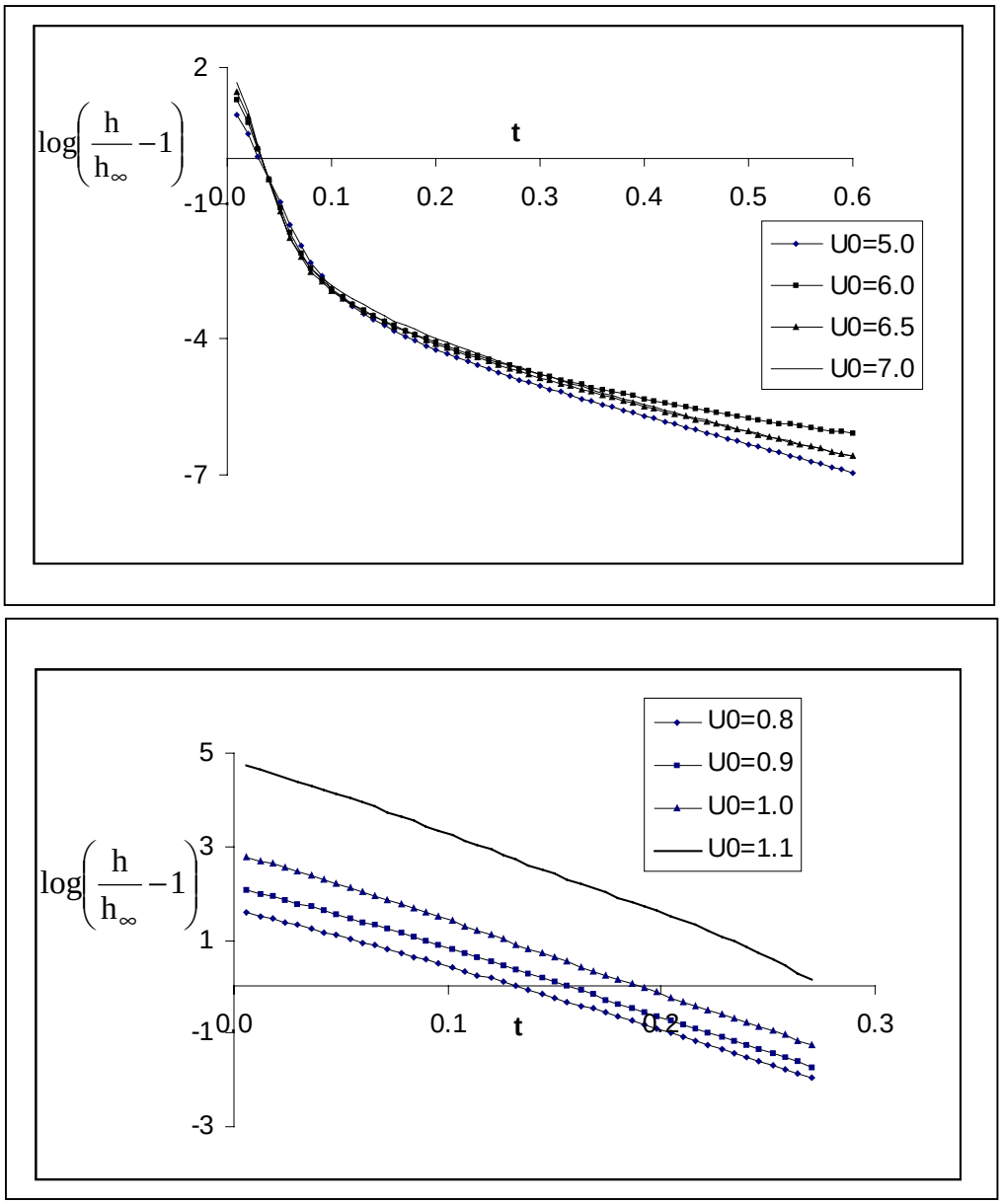

Figure 10 a and b.